

Ionospheric plasma acceleration at Mars: ASPERA-3 results

R. Lundin^{a,*}, D. Winningham^b, S. Barabash^a, R.A. Frahm^b, H. Andersson^a, M. Holmström^a, A. Grigoriev^a, M. Yamauchi^a, H. Borg^a, J.R. Sharber^b, J.-A. Sauvaud^c, A. Fedorov^c, E. Budnik^c, J.-J. Thocaven^c, K. Asamura^d, H. Hayakawa^d, A.J. Coates^e, D.R. Linder^e, D.O. Kataria^f, C. Curtis^f, K.C. Hsieh^f, B.R. Sandel^f, M. Grande^g, M. Carter^g, D.H. Reading^g, H. Koskinen^h, E. Kallio^h, P. Riihelä^h, W. Schmidt^h, T. Säles^h, J. Kozyraⁱ, N. Krupp^j, J. Woch^j, M. Fränz^j, J. Luhmann^k, S. McKenna-Lawler^l, R. Cerulli-Irelli^m, S. Orsini^m, M. Maggi^m, E. Roelofⁿ, D. Williamsⁿ, S. Liviⁿ, P. C:son Brandtⁿ, P. Wurz^o, P. Bochsler^o

^a Swedish Institute of Space Physics, Box 812, S-98 128, Kiruna, Sweden

^b Southwest Research Institute, San Antonio, TX 7228-0510, USA

^c Centre d'Etude Spatiale des Rayonnements, BP-4346, F-31028 Toulouse, France

^d Institute of Space and Astronautical Science, 3-1-1 Yoshinodai, Sagamichara, Japan

^e Mullard Space Science Laboratory, University College London, Surrey RH5 6NT, UK

^f University of Arizona, Tucson, AZ 85721, USA

^g Rutherford Appleton Laboratory, Chilton, Didcot, Oxfordshire OX11 0QX, UK

^h Finnish Meteorological Institute, Box 503, FIN-00101 Helsinki, Finland

ⁱ Space Physics Research Laboratory, University of Michigan, Ann Arbor, MI 48109-2143, USA

^j Max-Planck-Institut für Sonnensystemforschung, D-37191 Katlenburg-Lindau, Germany

^k Space Science Laboratory, University of California in Berkeley, Berkeley, CA 94720-7450, USA

^l Space Technology Ltd., National University of Ireland, Maynooth, Co. Kildare, Ireland

^m Istituto di Fisica dello Spazio Interplanetari, I-00133 Rome, Italy

ⁿ Applied Physics Laboratory, Johns Hopkins University, Laurel, MD 20723-6099, USA

^o Physikalisches Institut, University of Bern, CH-3012 Bern, Switzerland

Received 11 April 2005; revised 22 August 2005

Available online 10 February 2006

Abstract

The Analyzer of Space Plasma and Energetic Atoms (ASPERA) on-board the Mars Express spacecraft (MEX) measured penetrating solar wind plasma and escaping/accelerated ionospheric plasma at very low altitudes (250 km) in the dayside subsolar region. This implies a direct exposure of the martian topside atmosphere to solar wind plasma forcing leading to energization of ionospheric plasma. The ion and electron energization and the ion outflow from Mars is surprisingly similar to that over the magnetized Earth. Narrow “monoenergetic” cold ion beams, ion beams with broad energy distributions, sharply peaked electron energy spectra, and bidirectional streaming electrons are particle features also observed near Mars. Energized martian ionospheric ions (O^+ , O_2^+ , CO_2^+ , etc.) flow in essentially the same direction as the external sheath flow. This suggests that the planetary ion energization couples directly to processes in the magnetosheath/solar wind. On the other hand, the beam-like distribution of the energized plasma implies more indirect energization processes like those near the Earth, i.e., energization in a magnetized environment by waves and/or parallel (to B) electric fields. The general conditions for martian plasma energization are, however, different from those in the Earth's magnetosphere. Mars has a weak intrinsic magnetic field and solar wind plasma may therefore penetrate deep into the dense ionospheric plasma. Local crustal magnetization, discovered by Acuña et al. [Acuña, M.J., Connerey, J., Ness, N., Lin, R., Mitchell, D., Carlsson, C., McFadden, J., Anderson, K., Rème, H., Mazelle, C., Vignes, D., Wasilewski, P., Cloutier, P., 1999. *Science* 284, 790–793], provide some dayside shielding against the solar wind. On the other hand, multiple magnetic anomalies may also lead to “hot spots” facilitating ionospheric plasma energization. We discuss the ASPERA-3 findings of martian ionospheric ion energization and present evidences for two types of plasma energization processes

* Corresponding author.

E-mail address: rickard.lundin@irf.se (R. Lundin).

responsible for the low- and mid-altitude plasma energization near Mars: magnetic field-aligned acceleration by parallel electric fields and plasma energization by low frequency waves.

© 2005 Elsevier Inc. All rights reserved.

Keywords: Mars, atmosphere; Ionospheres; Magnetospheres

1. Introduction

Energization and escape of ionospheric plasma from the inner planets in the Solar System is the result of external forcing by the expanding solar corona plasma—the solar wind. For a strongly magnetized planet like the Earth the solar wind forcing is indirect, direct penetration of solar wind plasma to the upper atmosphere/ionosphere only taking place in two narrow dayside region—the polar cusps. Weakly magnetized planets like Venus and Mars behave more like comets, the entire dayside atmosphere/ionosphere representing a target for solar wind forcing, directly transferring energy and momentum to the ionosphere (e.g., [Luhmann and Bauer, 1992](#)). Solar wind forcing of a planetary atmosphere/ionosphere leads to loss of planetary matter, a planetary wind. The processes leading to such losses are essentially the same for all non-magnetized objects, including the more visible losses observed in the tail of comets. The question is rather, how different are the escape processes between magnetized and non-magnetized objects?

The escape and total loss of planetary volatiles from Mars has been subject for discussions ever since the confirmation of a “dry” planet in the late 1960 and early 1970. Various reasons for water drainage have been proposed such as catastrophic impact, Jeans escape and hydrodynamic escape (e.g., [Melosh and Vickery, 1989](#); [Chassifiere, 1996](#); [Kerr and Wetter, 2000](#)). In addition non-thermal escape due to solar wind forcing has been proposed (e.g., [McElroy et al., 1977](#); [Pérez-de-Tejada, 1987](#); [Luhmann and Bauer, 1992](#)). Based on the ASPERA findings from Phobos-2 ([Lundin et al., 1989](#)) the non-thermal ion escape was estimated to ≈ 1 kg/s. The ion composition of the non-thermal ion escape at Mars, the planetary wind, is a mix of O^+ and ionized molecules such as O_2^+ and CO_2^+ ([Norberg et al., 1993](#)). The major portion of the outflow was found to have energies below a few hundred eV, the outflow concentrated along the flanks of the martian tail ([Lundin and Dubinin, 1992](#)). On the other hand, observations in the central tail of Mars, the plasma sheet, frequently displayed ions beams accelerated up to several keV (e.g., [Lundin et al., 1990](#); [Verigin et al., 1991](#)). The central tail of Mars is therefore of particular interest with regard to the acceleration of plasma.

The plasma tail of a “non-magnetized” planet like Mars contains a mix of planetary and solar wind plasma, with a strong preference of planetary plasma in the inner tail ([Lundin et al., 1989, 1990](#)). This suggests that the induced magnetic field of a non-magnetized planet provide some shielding against solar wind penetration, at least in the nightside-tail region. However, the induced magnetic shielding appears to be less effective in the dayside and flank regions. The solar wind can penetrate deep into the dayside ionosphere, down to some 270 km altitude ([Lundin et al., 2004](#)). The solar wind is also effectively inter-

acting directly or indirectly with ionospheric plasma along the entire flanks of the induced magnetosphere of Mars, especially inside what has been termed the mass-loading boundary (e.g., [Lundin et al., 1991](#)). Notice that the mass-loading boundary is not synonymous with the magnetic pile-up boundary, MPB ([Vignes et al., 2000](#)), or the induced magnetosphere boundary, IMB ([Lundin et al., 2004](#)). IMB is defined as the envelope of the induced martian magnetosphere, marking a stopping boundary for solar wind plasma, the interior dominated by plasma of planetary origin. We note that this is only partly true because of the temporary access of solar wind plasma inside IMB ([Lundin et al., 2004](#)). Although the MPB (from B-field) and IMB (from particles) are conceptually different, they may yet represent the same boundary in space. On the other hand, the mass-loading boundary represents a smooth sheath transition region lying outside of MPB/IMB. Inside the mass-loading boundary the sheath plasma show signatures of heavy mass-loading, i.e., a gradual velocity decrease inwards ([Lundin et al., 1991](#)). From a kinetic point of view mass loading represents a direct or indirect transfer of energy and momentum from the solar wind to the planetary plasma ([Pérez-de-Tejada, 1987, 1998](#)). Such a kinetic approach is useful for the overall energy and momentum transfer, but it does not provide any details of the process that leads to such a direct or indirect forcing.

Localized energization and loss processes such as wave-particle interaction and quasi-static electric fields are well known in the Earth’s magnetosphere (see, e.g., book edited by [Paschmann et al., 2002](#)). The question is, do similar processes take place in the martian plasma environment? Furthermore, does the induced magnetic field, or the crustal magnetic play a role in the plasma energization at Mars?

The crustal magnetic field at Mars is an intriguing phenomena ([Acuña et al., 1999](#)). The field strength is apparently sufficient to magnetize the ionospheric plasma and to enable plasma access and energization processes like those above the Earth. The crustal magnetic field at Mars provide localized dayside shielding fending off the solar wind, but leaves at the same time open throats (cusps) where solar wind have focused access ([Krymskii et al., 2002](#); [Brain et al., 2005](#)). In the latter case a magnetized ionospheric plasma is subject to localized external forcing, the diverging magnetic field geometry facilitating upward energization and outflow of ionospheric plasma. The scattered multipole surface magnetic field at Mars therefore acts as both protection against and site for ionospheric plasma outflow ([Brain et al., 2005](#)), the net global effect for the outflow yet to be determined. Magnetic flux tubes from martian magnetic anomalies swept tailward by the solar wind ([Mitchell et al., 2001](#)) should also play a role in the energization and outflow of ionospheric plasma ([Brain et al., 2005](#)). Here again a diverg-

ing magnetic field provides an analogy with the energization of ionospheric plasma near the Earth.

Finally the external magnetic field, the solar magnetic flux pile-up, influences the energization and outflow of ionospheric plasma from Mars. Again the magnetic field, this time the draped magnetic field bordering Mars, provides an obstacle as well as a locus for plasma energization. Ideally, and in close proximity to the planet, the solar wind induced magnetic field is an obstacle for direct solar wind penetration. However, in reality the magnetic flux tubes swept tailward by the solar wind are turbulent and contain strong wave activity. Moreover, the IMF will control the rate of ion pick-up in the magnetosheath and tail for Mars (Luhmann and Schwingshuh, 1990; Sauer and Dubinin, 2000), in a similar manner as that discussed for Venus (Phillips et al., 1987; Slavin et al., 1989).

Solar wind magnetic field- and pressure irregularities may also lead to instabilities at the dayside contact surface that propagates deep into the martian ionosphere. The sheath plasma contains strong wave activity (Grard et al., 1989; Russell et al., 1990; Trotignon et al., 1996), waves that may propagate down to the ionosphere, leading to subsequent heating/energization of ionospheric plasma.

The dayside ionosphere of Mars is heavily bombarded by solar wind plasma leading to an energization of ionospheric plasma up to keV energies at low altitudes (Lundin et al., 2004). This raises the question: how can heavy ions reach so high energies at these low altitudes? What processes can possibly govern such acceleration? There is no immediate analogy with the Earth's topside ionosphere because the energization regions at Mars appears to be spatially more confined than those near the Earth. We will briefly address that issue in view of the ASPERA-3 findings above the dayside ionosphere of Mars.

ASPERA-3 observations of energized plasma along the flank and nightside/tail of Mars are more analogous with observations near the Earth. Signatures in the ion and electron data suggest plasma heating by waves as well as plasma acceleration in quasi-static electric fields. Indeed, the outflowing ionospheric plasma display electron and ion characteristics similar to those found in the topside ionosphere of the Earth. This suggests that plasma energization at the weakly magnetized Mars is coupled to ambient magnetic fields, the large-scale induced magnetic field and/or the crustal magnetic field.

2. ASPERA-3 observations of dayside plasma energization

The ASPERA-3 experiment (Barabash et al., 2004) has two plasma instruments, an Electron Spectrometer (ELS) and an Ion Mass Analyzer (IMA). ELS provides electron measurements in the energy range 0.001–20 keV with 8% energy resolution. The intrinsic field of view is $4^\circ \times 360^\circ$. The 360° aperture is divided into 16 sectors. The sensor consists of a top hat electrostatic analyzer in a very compact design. ELS is an improved version of the MEDUSA experiment (less the ion analyzer) for the Astrid-2 and Munin missions launched in 1998 and 2000. Both the ELS and IMA field of view covers roughly the solar and anti-solar direction along the s/c orbit. A solar/anti-solar coverage is ensured by electrostatic scanning

for IMA, while for ELS the 3D-coverage is obtained by implementing mechanical scanning.

IMA is an improved version of the ion mass spectrographs TICS/Freja, IMIS/Mars-96, IMI/Planet-B, and almost identical with the ICA instrument on ESAs Rosetta mission. IMA provides ion measurements in the energy range 0.01–30 keV/Q for the main ion components H^+ , He^{2+} , He^+ , O^+ , and the group of molecular ions ($20 < M/q < \sim 80$). IMA has a $4.6^\circ \times 360^\circ$ field of view. Electrostatic sweeping performs elevation ($\pm 45^\circ$) coverage, thus providing a total field of view of about 2π . The elevation sweeping is the main cause of modulations appearing in the energy–time spectrograms of Figs. 2, 4, 5, and 9.

The IMA sensitivity for low-energy ions is reduced in the angular sweeping mode. Ions less than about 300 eV are usually below the measurement threshold, except when encountering the dense martian ionosphere. An energy–mass matrix with IMA data from the dayside pericenter is shown in Fig. 1. The figure shows a mix of cold ionospheric O_2^+ , energized O^+ (and O_2^+), and penetrating solar wind ions (H^+ and He^{2+}). Notice that cold ionospheric ions such as those observed in Fig. 1 can only be measured in the s/c ram-direction ($v_{sc} > 6$ km/s).

Phobos-2 results indicated that energized planetary ions flows tailward, essentially in the same direction as the external sheath flow (Kallio et al., 1994). A tailward flow appears to start at low altitudes (< 1000 km). This resembles morphologically the solar wind interaction with a comet, indicating a mass loaded pick-up process commencing at low altitudes, continuing out to the mass-loading boundary. An energization described by single particle motions in the solar wind electric and magnetic-field appears to be valid only at large distances from the planet, outside the mass-loading boundary (Lundin and Dubinin, 1992). ASPERA-measurements on Phobos-2 also indicated that the planetary wind gradually approaches solar wind velocities in the deep tail (Lundin et al., 1991). The low-altitude tailward flow of planetary ions in the early energization phase was confirmed by ASPERA-3 on Mars Express (Lundin et al., 2004).

Fig. 2 shows an ASPERA-3 energy–time ion and electron spectrogram from a dayside pericenter (297 km) pass near local noon. The MEX s/c enters the martian dayside magnetosphere from the northern hemisphere sheath, crossing the induced magnetosphere boundary (IMB), minutes later traversing the photoelectron boundary (PEB). The existence of photoelectrons during 10:23–10:34 UT, indicated by the intensification at ≈ 20 eV, is evidence for ionospheric electrons. During outbound the s/c again traverse PEB and IMB and enters the dayside southern hemisphere sheath. Notice that solar wind ions, H^+ and He^{2+} , (top panel) penetrated down to pericenter altitudes, i.e., this dayside region down to some 300 km altitude was subject to direct solar wind forcing. Concurrent energization of ionospheric heavy ions (panel 2) takes place throughout this dayside pass. The average heavy ion energy spectrum accumulated during 15 min peaks at ≈ 800 eV and has a characteristic energy/temperature of 230 eV. The solar wind proton spectrum has a somewhat higher peak energy and temperature. A difference in flow direction between solar wind and planetary ions up to 60° is observed during this pericenter pass.

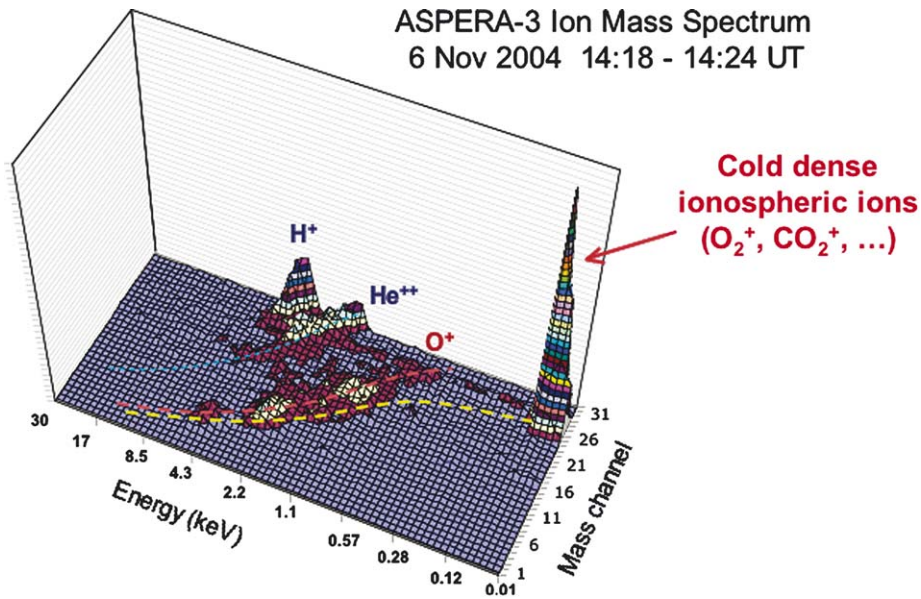


Fig. 1. IMA energy–mass spectrogram with cold ions detected while ramming the dense Mars ionospheric plasma. Colored lines mark mass lines for He^{2+} , O^+ and O_2^+ . Notice that H^+ ions in this post-acceleration mode are cut off at energies below ≈ 2 keV.

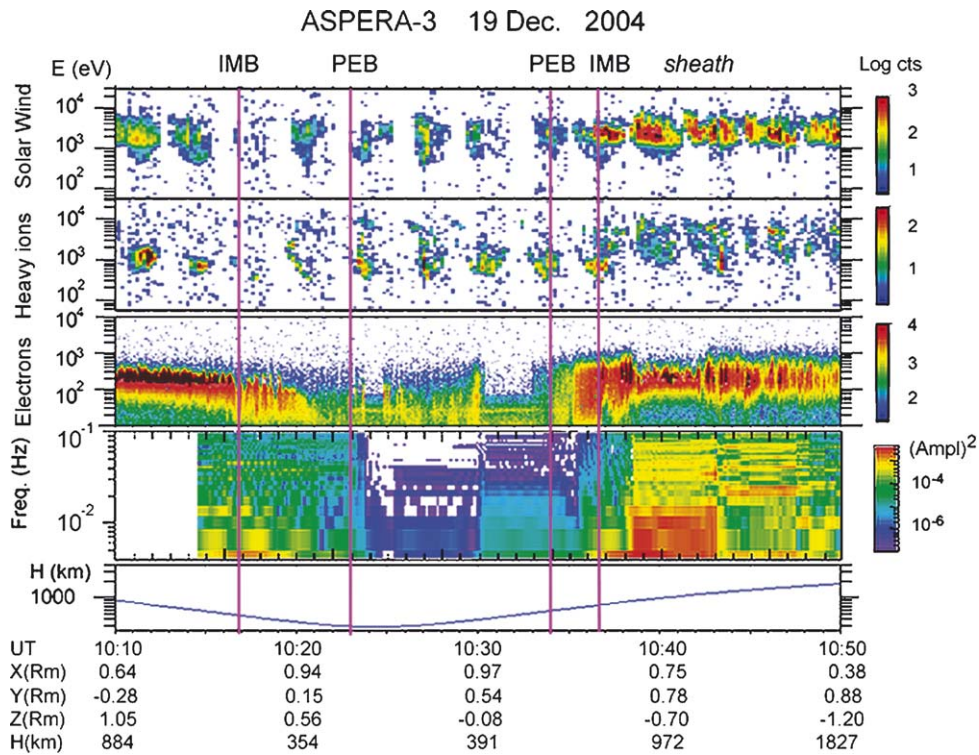


Fig. 2. Energy–time spectrogram of ions and electrons (top three panels) and electron frequency spectra (bottom panel) from a dayside pericenter (297 km) pass near local noon, 19 Dec. 2004, illustrating the presence of solar wind and energized heavy ions down to the spacecraft pericenter. The IMB and PEB boundaries are marked out (see text).

The difference may be attributed to external solar wind forcing of the magnetized plasma, the ionospheric ions rendering a more upward motion from the planet, perhaps associated with the crustal magnetic field.

The enhanced temperature of the planetary ions suggests strong local wave heating. The heating must be rapid in view of the low altitude of the observation. A similar finding was

made near the Venus ionopause (Shefer et al., 1979), suggesting rapid plasma heating in the upper ionosphere of both Mars and Venus. The two bottom panels display ELS-data for downgoing electrons, the bottom panel showing FFT spectra for electrons in the frequency range 10^{-1} – 4×10^{-3} Hz. The high-time resolution data from ELS shows clear evidence of wave activity that may be attributed to plasma energization (Winningham et

Table 1
MEX dayside pericenter traversals of regions with planetary ion energization

Date	Time (UT)	E_m (eV)	T_c (eV)	H_p (km)	H_{sw} (km)	Long (deg)
2004-10-17	10:30–10:55	600	1500	270	560	–20
2004-11-12	11:25–11:30	600	700	280	400	–158
2004-12-17	18:05–18:10	1400	2500	300	330	–60
2004-12-18	00:40–00:55	700	790	300	300	–38
2004-12-19	10:15–10:40	800	231	300	300	–170
2004-12-20	06:20–06:45	530	160	300	300	–104
2005-01-21	11:15–11:35	600	180	300	300	–105

E_m = planetary ion peak energy, T_c = planetary ion temperature, H_p = min. altitude for planetary ion energization, H_{sw} = min. altitude of penetrating solar wind ions, Long = geographic longitude of the traversal.

al., 2006). The wave amplitude peaks at low frequencies, but several resonance features at higher frequencies may also be observed as discussed by Winningham et al. (2006). Using MGS magnetic field data Espley et al. (2005) found low-frequency oscillations in the same frequency range, near the O^+ gyrofrequency. It is feasible to associate the electron flux variability in Fig. 2 with electromagnetic waves in the oxygen cyclotron frequency range. Low frequency fluctuations of electrons such as those observed here may therefore represent the “smoking gun” of local wave-heating of ionospheric O^+ and molecular ions such as O_2^+ and CO_2^+ , the waves associated with solar wind plasma forcing.

Intense wave activity may also have an impact on the momentum transport between the solar wind plasma and the ionospheric plasma as suggested by Shapiro et al. (1995). The wave activity should go into calculations of the viscosity and thermal conductivity terms describing the momentum transport as discussed by Pérez-de-Tejada (2005). In this way intense wave activity may also lead to enhanced bulk outflow of ionospheric plasma.

Table 1 summarizes data from 7 dayside pericenter passes with planetary ion energization down to pericenter altitudes. In four of the cases the solar wind plasma penetrated down to the pericenter (≈ 300 km). Notice that the characteristic energies of the energized ionospheric heavy ions varied from 160–2500 eV—corresponding to a raise of ion temperature from <1 eV to hundreds of eV in close proximity of a cold and dense ionosphere!

3. ASPERA-3 observations of flank and tail plasma energization

A detailed analysis has been made of data from 25 selected MEX orbits with plasma energization along the flanks and in the plasma tail of Mars. The orbit selection was based on an adequate coverage of the ion outflow. Fig. 3 shows orbit trajectories with planetary ion outflow for the 25 orbits, the orbit tracks projected in a cylindrical coordinate system. In most cases the ion outflow is in the direction of the external solar wind/sheath flow, the exceptions mainly located at low altitudes near the subsolar region. The figure illustrates that energized ion outflow may be observed within the entire tail out to the induced magnetosphere boundary (IMB), the IMB here referring to the average “MP” boundary deduced from Phobos-2

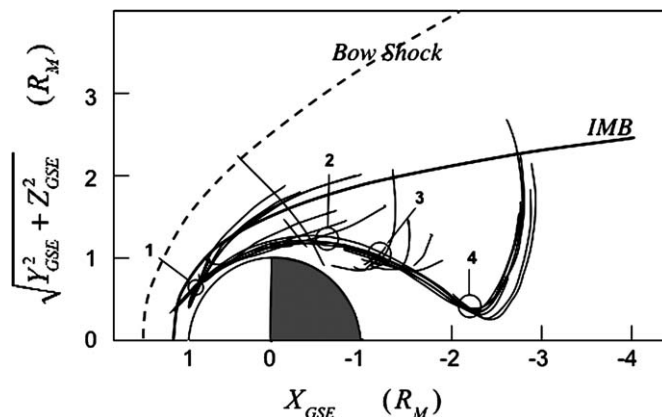


Fig. 3. Morphology of the planetary ion acceleration and outflow. MEX trajectory traces with observations of ion acceleration and outflow are depicted using a cylindrical coordinate system. IMB marks the average induced magnetosphere boundary. The position of the traversals shown in Figs. 2, 4, 5 and 9 are marked out by circles. 1 = Fig. 2 (10:25 UT, pericenter); 2 = Fig. 4 (12:56 UT, single spectra); 3 = Fig. 5 (10:53 UT); 4 = Fig. 9 (06:53 UT).

data (e.g., Lundin et al., 1991). Numbered circles represent orbit locations of the four examples considered in more detail in this report. The ion outflow may be divided in two categories: (a) broad-energy hot ion beam, and (b) monoenergetic cold ion beams.

The first category (a) display a feature observed in the terrestrial ion outflow. A broad ion energy distribution is in the terrestrial case associated with energization/heating by waves. Studies in the Earth’s magnetosphere shows that waves play an important role in energizing space plasmas (see, e.g., Moore et al., 1999, for a review). However, for heating/energization to result in a beamed outflow, a plasma anisotropy, an ambient magnetic field, is required. The diverging magnetic dipole field of the Earth represents such an anisotropy, the gradient ($\nabla_{\parallel} B$) facilitating outward directed ponderomotive acceleration (e.g., Guglielmi and Lundin, 2001). Near Mars, the induced magnetic field or/and magnetic anomalies provide an anisotropy sufficient for a directed outflow. Moreover, the tailward flaring magnetic field is further support for divergence in support for wave-induced ponderomotive forcing.

The second category (b) is strikingly similar to the monoenergetic ion outflow observed over the Earth’s auroral zone, ion beams associated with magnetic field-aligned electric field acceleration. Concurrent with electric field (upward) ion acceleration is a corresponding opposite (downward) acceleration of electrons. The direction of charged particle beams, negative and positive charges flowing in opposite directions, gives the direction of the electric field. Oppositely flowing ions and electrons also suggests a net electric (field-aligned?) current.

Fig. 4 illustrates the first category (a), outflowing ions with a broad energy distribution. The left panel display energy–time spectrograms for heavy ions (top), down-going electrons (middle), and frequency spectra of electrons (bottom). The two panels to the right show ion and electron spectra for the time period 12:56–13:03 UT. During this pass MEX reaches pericenter on the nightside with ion energization observed in the tail lobe and in the flanks. The ion and electron spectrum panels

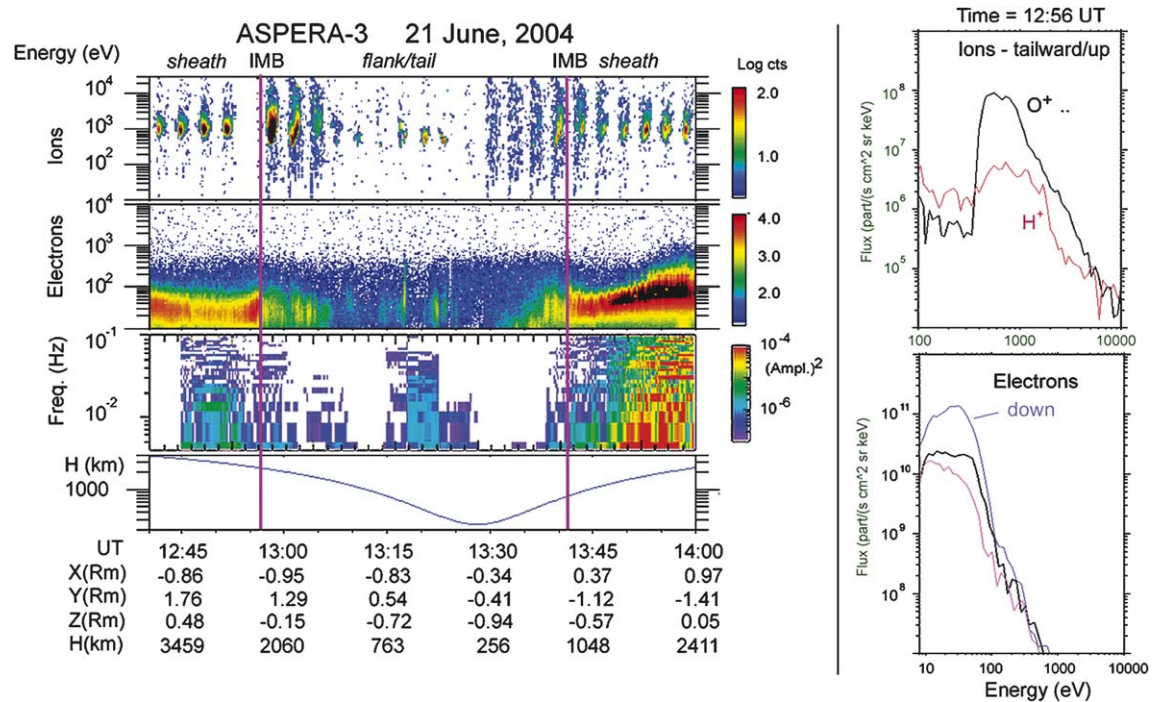


Fig. 4. IMI and ELS data from a MEX pericenter pass on June 21, 2004, the eclipse marked by dashed square. The upper diagram shows data (counts) of tailward moving planetary ions ($m/q = 16\text{--}44$ amu). The middle panels display down-going electron energy spectra (counts) and the frequency spectra of electrons, respectively, and the lower panel the altitude above the planetary surface. IMB marks the induced magnetosphere boundary. The ion and electron flux spectra to the right are taken at 12:56 UT.

(at 12:56 UT) correspond to the orbital location 2 in Fig. 3. We note here the simultaneous outflow of planetary H^+ and heavy ions (dominated by O^+). The mean energy and temperature of the O^+ beam is ≈ 600 and ≈ 260 eV, respectively, illustrating that cold ionospheric ions may be strongly heated in the course of the escape—from less than an eV to hundreds of eV. Notice that the heavy ion-beam also contain molecular ions (e.g., O_2^+). The individual species temperatures are somewhat lower than 260 eV since there is a tendency for the energization to be mass-dependent, heavier ions reaching higher energies. Unless a strong magnetic folding can be inferred, not likely for Mars, the ≈ 600 eV average beam energy cannot be explained by ion heating only. Electric field acceleration, as discussed later, may have to be inferred as well.

The spectra for downgoing electrons (sectors 8, 9) illustrates a feature found in connection with ion heating above the Earth's auroral zone, high fluxes of streaming electrons. The temperature of the streaming electrons is relatively low, ≈ 11 eV, indicating little or no heating of electrons. Notice also the variability of the electron fluxes associated with ion heating, with frequencies in the 5–30 mHz range. We believe these variations reflect the ion heating process, the frequency being in the neighborhood of the oxygen and molecular ion cyclotron frequencies (Winningham et al., 2006).

Fig. 5 shows an example of the second category (b), monoenergetic ion beams. The left panel shows energy–time spectrograms of heavy ions and electrons, and the right-hand side panels energy spectra for ions and electrons at 10.53 UT. This time the ion outflow, corresponding to the orbital location 3 in Fig. 3. ($\approx 10:45\text{--}11:00$ UT), is observed just inside the eclipse

region. The H^+ and O^+ spectra are clearly monoenergetic, the O^+ ions having somewhat higher peak energy. The ion beam energy and temperature were ≈ 1500 and 130 eV, respectively. Some heating of the ionospheric ions is apparently present in this case as well. However, it is by comparing ions and electrons that the most revealing information is obtained. First of all, the ELS data show strong low-frequency modulations with a peak at 20 mHz (third panel). This suggests that the ions are heated by waves. Notice the ≈ 120 eV energy peak in the downgoing electrons, with low fluxes at low energies. Peaked electron and ion energy spectra suggest a mono-energetic acceleration processes. Moreover, ion and electron acceleration in magnetic field-aligned electric fields leads to oppositely flowing electron and ion beams, as well as electric currents. If this is the case the upgoing ion peak at 1500 eV implies a voltage of ≈ 1500 V below the s/c while the downgoing electrons implies an acceleration by ≈ 120 V above the s/c.

The lack of magnetic field data from MEX makes a pitch angle analysis quite difficult. The large-scale magnetic field may be inferred from the solar wind sweeping, the field lines swept tailward by the external solar wind forcing. More detailed magnetic field directions may be inferred in the future from a pressure analysis of the electron-data in the angular scanning mode of ASPERA-3. The data received so far give a 2D cut of the unit sphere, the magnetic field vector expected to be in the ELS measurement plane in the deep nightside tail. The electron data sometimes shows a loss-cone distribution, but due to spacecraft constraints a more detailed analysis of data is required before conclusions can be drawn from this. However, the general electron energy and angular distributions show fea-

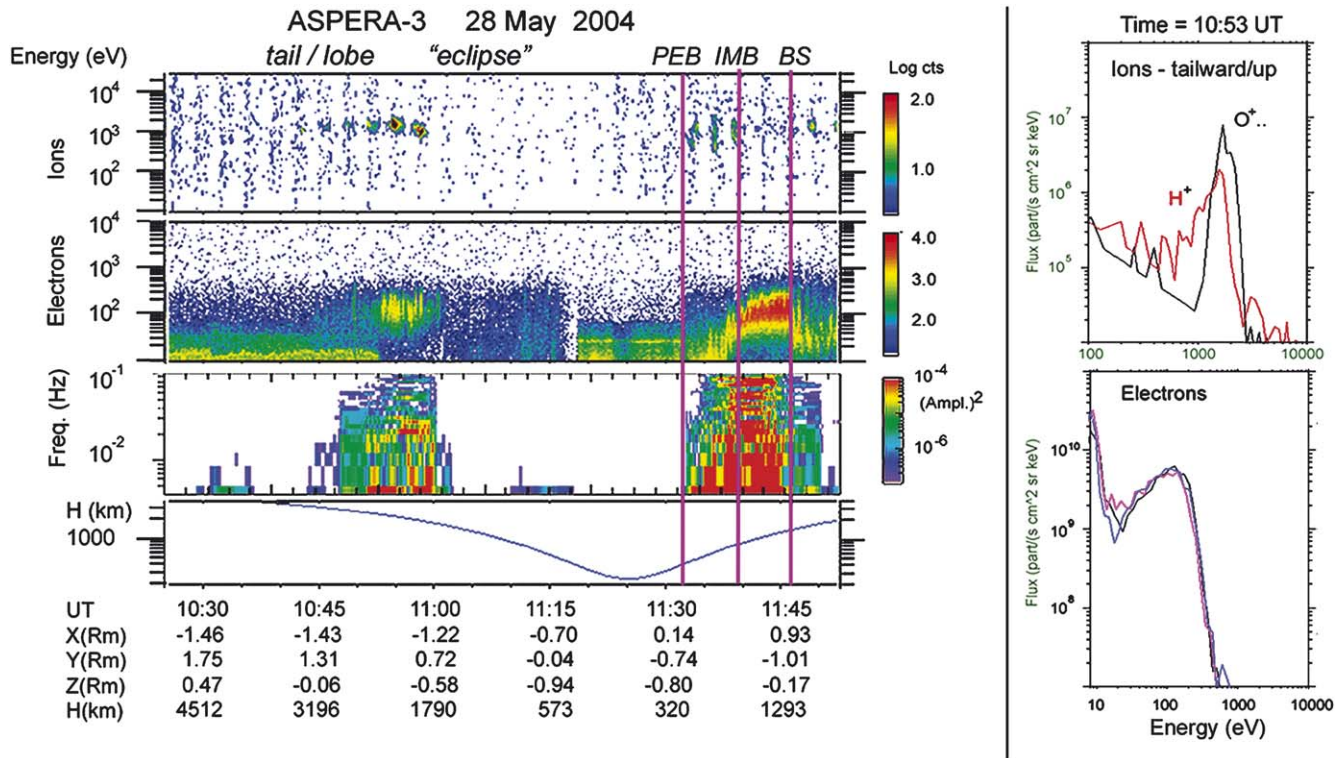


Fig. 5. IMI and ELS data from a MEX pericenter pass in May 28, 2004, the eclipse marked by dashed square. The format is the same as that in Fig. 4. Marked out are the s/c traversal of the PEB, IMB and BS (Bow Shock).

tures that are strikingly similar to those found in the Earth's auroral acceleration region. Moreover, the enhanced electron temperature in the beam, ≈ 48 eV suggests electron heating, potentially as a result of beam-broadening instabilities. Such instabilities are expected to occur in the field-aligned acceleration process as a result of bidirectional streaming, the incident electron beam meeting a return beam of electron caused by atmospheric backscattering and magnetic mirroring (see, e.g., review by Moore et al., 1999).

An account of the distribution of ion- and electron peak energies in the data set is shown in Figs. 6a and 6b, respectively. We have divided the peaks into “monoenergetic” and “hot beams” for ions, and “peaked” and “streaming” for electrons. Both “peaked” and “streaming” electrons are streaming in the sense unidirectional or bidirectional, the difference being that only “peaked” have distinct and narrow energy peaks. Notice that most ion peaks fall in the 500–1600 eV range. This reflects the selection criteria rather than the probability of finding ion energy peaks. A more extensive study is required to give the statistics of ion energy peaks. In a similar manner the electron peaks reflect the selection process. However, electron peaks are usually concurrent with ion peaks. Fig. 6b shows that electron peaks are observed up to >250 eV. The highest electron energy peak is about 450 eV in this data set. Notice in Fig. 6b the trend for peaked electron spectra to reach high energies. Conversely, streaming electrons have predominantly low peak energies.

Figs. 7a and 7b show beam temperatures for ions and electrons, respectively, using the above data set. Fig. 7a demonstrates that monoenergetic ions beams have preferentially low

temperatures (<120 eV) while the hot ion beams have high temperatures. The corresponding trend for electrons is the opposite, the peaked electron spectra having the highest temperatures.

In summary Figs. 6 and 7 demonstrate that:

- “monoenergetic” out-flowing ion beams have low ion temperatures and are associated with high temperature down-going peaked electrons;
- “hot beam” out-flowing ions have high ion temperatures, and are associated with low temperature streaming electrons.

The local time distribution of ion and electron beams is shown in Fig. 8, using the above categorization. As part of the selection criteria, most data points falls in the midnight sector, with scattered data points at other local times. We note from Fig. 8 that the highest electron beam energies (and the highest electron temperatures, not shown here) are found near local midnight. Whether this has any significance for the acceleration process as such, for instance if it is related with the crustal magnetic field on Mars, will be subject for another study. An example of upward–downward acceleration near local midnight in the eclipse region is shown in Fig. 9. The ion and electron spectrum panels (at 06:55 UT) correspond to the orbital location 4 in Fig. 3. Notice that the entire acceleration region is characterized by strong low-frequency wave activity. The electron and O^+ flux spectra peaks at ≈ 350 and ≈ 1100 eV, respectively, the electron peak now being very narrow. Notice that H^+ peaks at a lower energy than O^+ , suggesting that a mass-dependent accel-

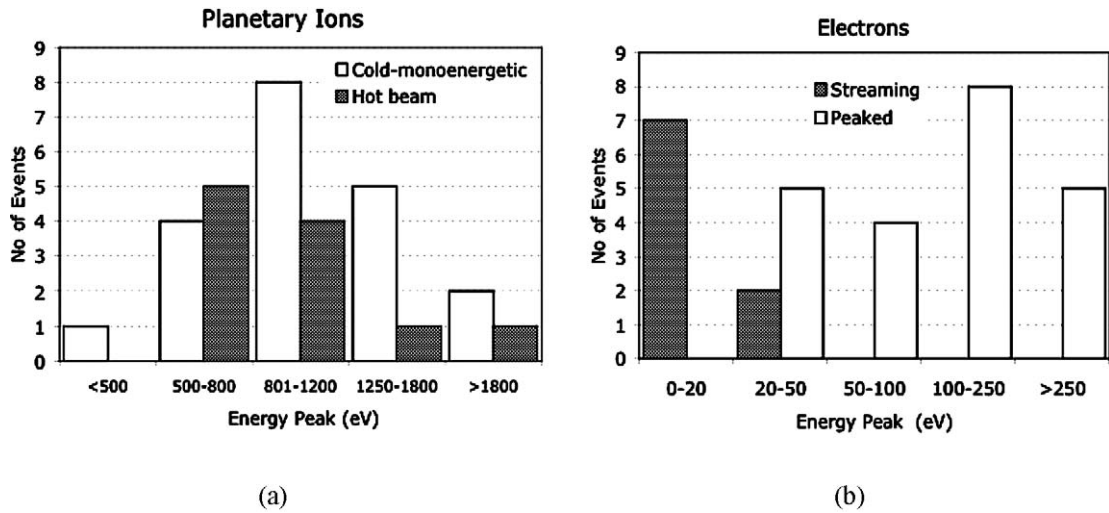


Fig. 6. Peak energies for planetary ions (a) and electrons (b) based on the categorization scheme described in the text.

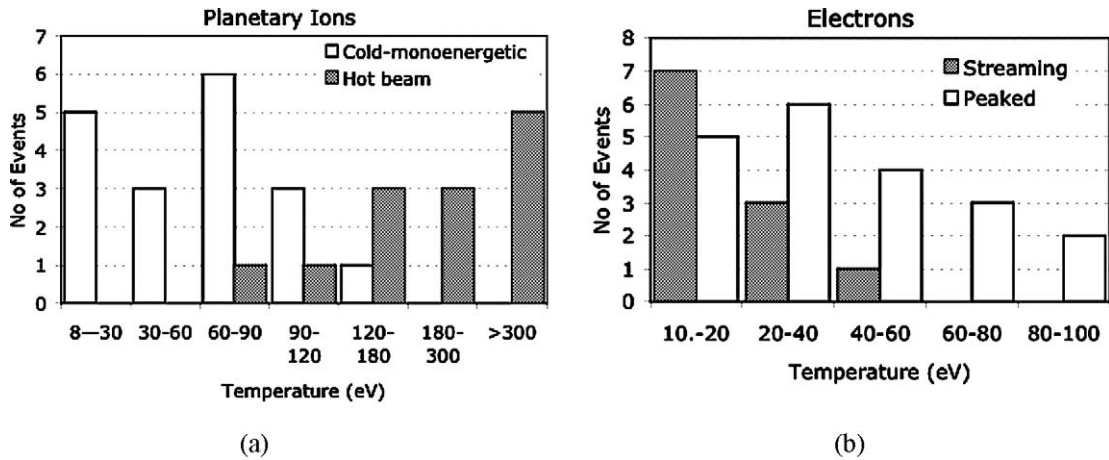


Fig. 7. Beam temperature for planetary ions (a) and electrons (b) based on the categorization scheme described in the text.

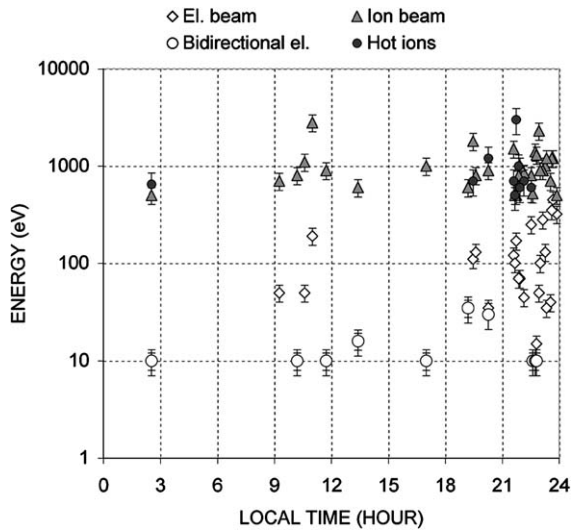


Fig. 8. Local time distribution of ion and electron energy peaks deduced from 31 IMA and ELS energization cases. Ion and electron “monoenergetic” beams tends to occur predominantly in the nightside (around 2400 LT) while heated ions and electrons are more widely distributed.

eration must be taken into account as well. The electron and ion beam temperatures are 79 and 75 eV, respectively. The similarity between these ion and electron spectra and those associated with field-aligned acceleration above the Earth’s auroral zone is indeed quite striking.

The altitude distribution of electron and ion beam energies in the midnight sector of Mars gives further evidence for an “auroral” acceleration process. In Fig. 10a ion and electron beam energies are plotted versus altitude in the midnight sector (21–24 LT). Depicted in Fig. 10a is also the total acceleration, adding ion and electron beam energies. Fig. 10b, displaying the relative contribution of ion acceleration to the total acceleration (ion acceleration/total acceleration), gives further support for the hypothesis that the acceleration is due to an altitude dependent electric field acceleration. Dashed line gives a power law fit to the data points. Although the correlation coefficient is rather low ($R^2 = 0.50$) the trend is yet that the ion acceleration contribution to the total acceleration (ions + electrons) decreases with height. This suggests that the electron acceleration may dominate at low altitudes near local midnight (where no data is available). The lack of accelerated electrons above

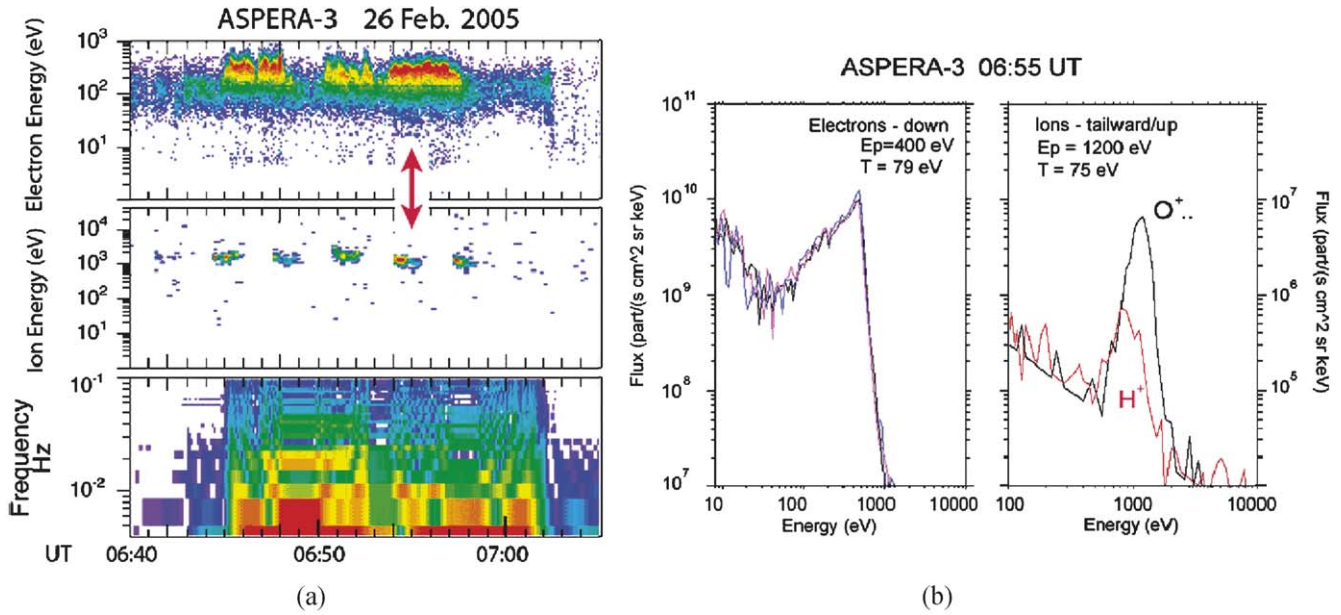


Fig. 9. (a) Energy–time spectrogram for electrons and ions during Feb. 26, 2005, showing plasma acceleration in the deep nightside. Except for the change of order of the two upper panels, the format is the same as in Figs. 4 and 5. (b) Energy spectra of oppositely accelerated electron and ion fluxes in the central tail at 06:55 UT (marked by red arrow in Fig. 9a).

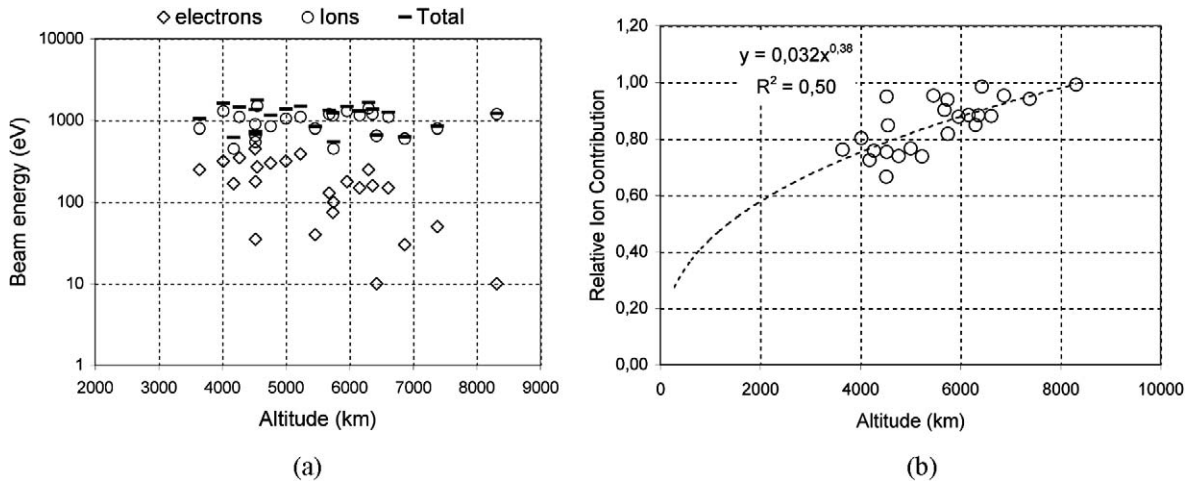


Fig. 10. Acceleration of ions and electrons above Mars, the data taken from the midnight sector (longitude $\approx 160^\circ$ – 180°). (a) Ion and electron beam energies versus altitude. “Total” marks the sum of the ion and electron beam energy. (b) Relative ion contribution to the total acceleration versus altitude. Dashed curve shows a power-law fit to the data with correlation coefficient 0.50.

≈ 8000 km suggests a height limited process. Drawing the analogy further with the Earth suggests precipitation of accelerated electrons (≈ 1 keV) into the nightside atmosphere of Mars. This leads to light emissions—aurora. The terminology “auroral” acceleration may therefore be adequate also for Mars.

4. Discussions

We have presented results from ASPERA-3 of the escape of ionospheric plasma from Mars, focusing on the energization of ions and electrons. Energization of ionospheric plasma is expected to result from a direct and/or indirect interaction with the solar wind. With direct interaction we mean that solar wind energy and momentum is transferred locally, i.e.,

ionospheric plasma is in direct “contact” with penetrating solar wind plasma. Direct interaction/forcing, leading to outflow and escape, may be described by simple kinetics (Pérez-de-Tejada, 1987), taking into account for mass loading (Lundin et al., 1991). Microphysical processes may also be described in forcing terms. The latter is relevant for indirect interaction, i.e., solar wind kinetic energy is converted to electromagnetic energy. Conversely, electromagnetic energy may propagate down to a planetary ionosphere and atmosphere, the wave energy converting back to particle kinetic energy.

The dayside and flank ionosphere of Mars is particularly exposed to direct solar wind scavenging, the solar wind sometimes reaching altitudes of 300 km or less (Fig. 2). An interesting aspect of direct solar wind contact with the ionosphere is the ener-

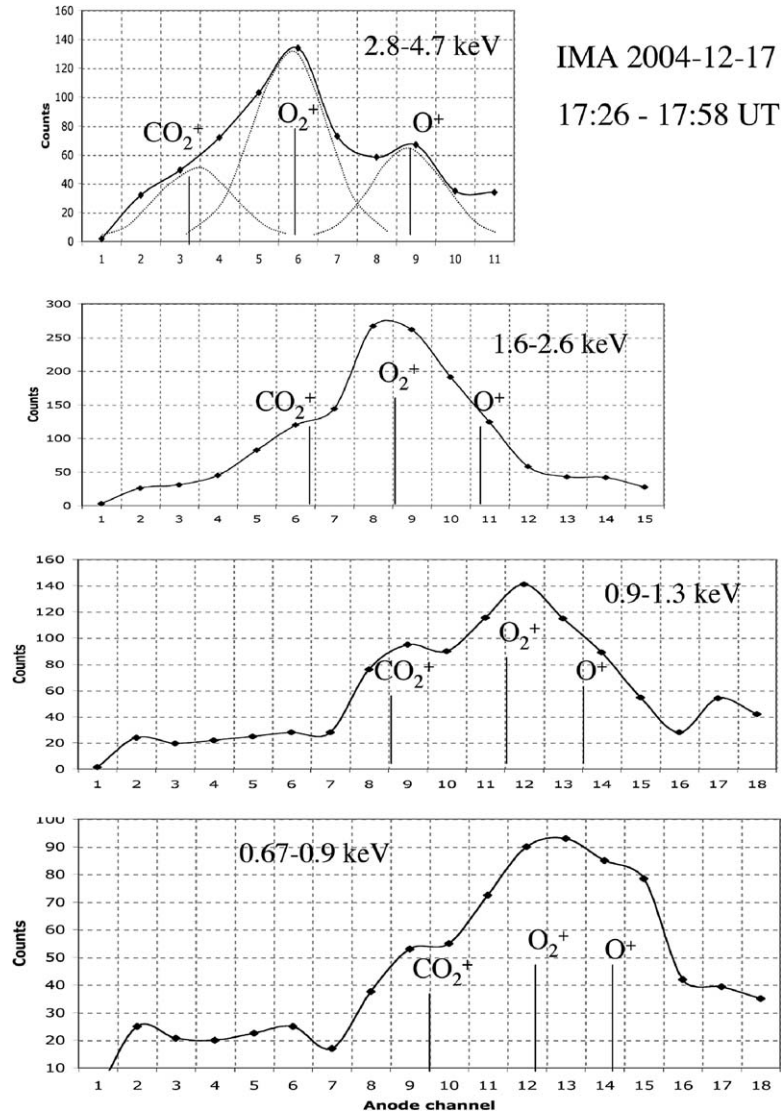


Fig. 11. Example of mass spectrum of O^+ ($m/q = 16$), O_2^+ ($m/q = 32$), and CO_2^+ ($m/q = 44$) ions for the energy interval 0.67–4.7 keV. The figure illustrates that the planetary outflow corresponds to a representative mix of ions from the martian ionosphere.

gization of planetary ions to energies in the keV-range (Lundin et al., 2004). Planetary ion beams from the dayside/flank are quite hot, in general hotter than nightside tail beams. Moreover, the direction of the planetary wind replicates well the external flow in the sheath, the shocked solar wind. This is suggestive of a rather direct solar wind energy and momentum transfer. On the other hand, the planetary wind may have a high ion temperature, frequently exceeding 200 eV that is well above the ionospheric temperature (< 1 eV). This indicates strong ion heating, presumably by waves, a heating that may occur at quite low altitudes, sometimes in confined regions.

Phobos-2 results indicated that the planetary ion outflow constituted a mix of O^+ and molecular ions (O_2^+ , CO_2^+ , etc.) (e.g., Norberg et al., 1993), but the mass resolution was insufficient to clearly separate the molecular species. The mass resolution on ASPERA-3 is better, so we can now really conclude (Karlsson et al., 2006) that the outflow is a representative mix of the martian upper atmosphere and ionosphere (Nier and McElroy, 1977; Hanson et al., 1977). Fig. 11 illustrates this,

a planetary ion outflow in the keV-range locally dominated by molecular O_2^+ and CO_2^+ . The latter is further support for an energization process extending deep into the martian ionosphere where molecular ions dominate.

Obvious regions at Mars with a magnetic field stretching into the central tail, and therefore potentially being connected with a tailward acceleration of ions and acceleration of electrons into Mars, are cusps associated with the magnetic anomalies at Mars (Acuña et al., 1999; Krymskii et al., 2002; Brain et al., 2005). One may conceive open magnetic flux tubes extending out from adjacent crustal magnetizations, harboring field-aligned currents and parallel electric fields. Fig. 12 is an illustration of such a connection between an acceleration region extending below some 8000 km (Fig. 9) down to the topside ionosphere and atmosphere of Mars. Such connectivity would also lead to intense electron precipitation and aurora. Recent findings from Mars Express (Bertaux et al., 2005) are evidence for airglow/aurora at Mars, but more detailed studies combining ASPERA-3 and SPICAM are required to resolve the issue

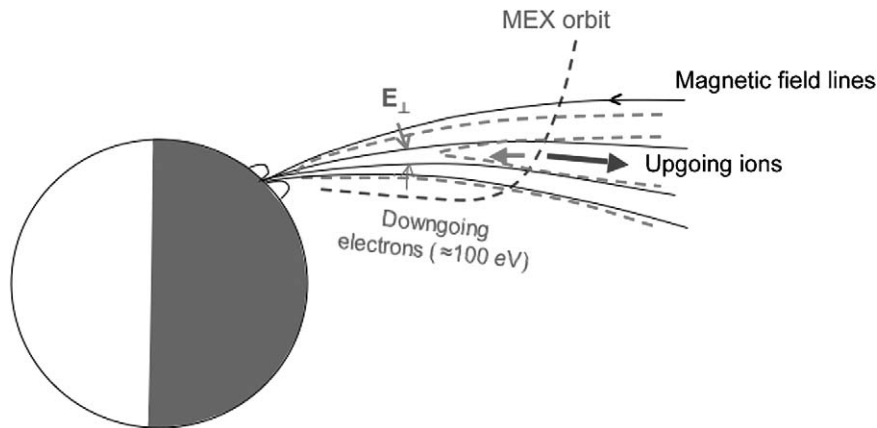


Fig. 12. Diagram illustrating ionospheric plasma escape by field aligned quasi-electrostatic fields (Figs. 5 and 9).

about aurora at Mars. Discrete aurora, if existing, is expected to occur in separation regions, cusps, between crustal magnetic field regions at Mars.

The plasma acceleration observed with ASPERA-3 near Mars have features that are strikingly similar to the Earth's auroral acceleration processes. ASPERA-3 data shows that "monoenergetic" ion outflow is associated with energized electrons, their peak energy gradually increasing with altitude. Features that adds to the complexity of the auroral acceleration process is also there, such as the tendency for high masses to become energized to higher energies (e.g., Collin et al., 1981). We also observe strong ion heating with almost no energization of the electrons. These are all features well known in terrestrial magnetospheric physics.

5. Conclusions

New data from ASPERA-3 on Mars Express have provided better data of solar wind forcing of the martian atmosphere and ionosphere. In this report we have focused on certain aspects of the solar wind forcing, such as:

- the energization and outflow of ionospheric ions;
- dayside and nightside differences in the energization process;
- the potential existence of aurora in the nightside region of Mars.

The energization and outflow of ionospheric plasma from Mars show strong similarities with the energization and escape of terrestrial ionospheric plasma, despite that Mars is a weakly magnetized planet. The crustal magnetic anomalies at Mars may play an important role for the plasma energization process, but the induced magnetic field of Mars must also be considered. Low-frequency wave activity generated by the shocked solar wind plasma near Mars and quasi-static electric fields comprise major forcing terms in the ion and electron energization process. Low frequency wave activity, here identified from electron fluctuations (Winningham et al., 2006), is detected almost everywhere in the martian magnetosphere, thus representing a more widespread source for plasma energization.

Acceleration and heating by low-frequency waves is primarily affecting ions, which is consistent with our observation. Simultaneous observations of electrons show marginal heating effects. Conversely, "field-aligned" plasma acceleration by presumably parallel electric fields, strongly affects both ions and electrons. This is consistent with ASPERA-3 observations in primarily the midnight sector. We propose that the field-aligned acceleration is related with "cusps" emerging from neighboring crustal magnetization regions. The "cusps" represents the magnetic foot-point of diverging magnetic flux tubes extending into the nightside of Mars. On a small scale the topology resembles the diverging magnetic field above the Earth's auroral oval as indicated in Fig. 12.

Acknowledgment

The ASPERA-3 experiment on the ESA Mars Express is a joint effort between 15 laboratories in 10 countries, all supported by their national agencies. We thank all these agencies, as well as the various department/institutes hosting these efforts. We wish to acknowledge in particular the Swedish National Space board supporting the main PI-institute, and NASA for its support of the main PI-institute. We are indebted to European Space Agency for their courage in embarking on MEX, the first ESA mission to the red planet.

References

- Acuña, M.J., Connerey, J., Ness, N., Lin, R., Mitchell, D., Carlsson, C., McFadden, J., Anderson, K., Rème, H., Mazelle, C., Vignes, D., Wasilewski, P., Cloutier, P., 1999. Global distribution of crustal magnetization discovered by Mars Global Surveyor MAG/ER experiment. *Science* 284, 790–793.
- Barabash, S., Lundin, R., Andersson, H., the ASPERA-3 team, 2004. The analyzer of space plasmas and energetic atoms (ASPERA-3) for the Mars Express mission. In: *Mars Express—The Scientific Payload*, ESA SP-1240.
- Bertaux, J.-L., Leblanc, F., Witasse, O., Quemerais, E., Lilensten, J., Stern, S.A., Sandel, B., Koalbeiv, O., 2005. Discovery of an aurora on Mars. *Nature* 435, 9.
- Brain, D., Luhmann, J., Mitchell, D., Lin, R., 2005. Expected influence of crustal magnetic fields on the ASPERA-3 ELS observations: Lessons learnt from MGS. In: *1st Mars Express Science Conference*, 21–25 Feb. 2005. <http://sci.esa.int/science-e/www/object/index.cfm?fobjectid=36537>.

- Chassifiere, E., 1996. Hydrodynamic escape of oxygen from primitive atmospheres: Application to the cases of Venus and Mars. *Icarus* 124, 537–552.
- Collin, H.L., Sharp, R.D., Shelley, E.G., Johnson, R.G., 1981. Some general characteristics of upflowing ion beams over the auroral zone and their relationship to auroral electrons. *J. Geophys. Res.* 86, 6820–6826.
- Espley, J.R., Cloutier, P.A., Crider, D.H., Brain, D.A., Acuna, M.H., 2005. Low frequency oscillations at Mars during the October 2003 solar storm. *J. Geophys. Res.* 110, doi:10.1029/2004JA010935. A09S33.
- Grard, R., Pedersen, A., Klimow, S., Savin, S., Skalsky, A., Trotignon, J.G., Kennel, C., 1989. First measurements of plasma waves near Mars. *Nature* 341, 607–609.
- Guglielmi, A., Lundin, R., 2001. Ponderomotive upward acceleration of ions by ion-cyclotron and Alfvén waves over the polar regions. *J. Geophys. Res.* 106, 13219–13236.
- Hanson, W.B., Sanatani, S., Zuccaro, D.R., 1977. The martian ionosphere as observed by the Viking retarding potential analyzer. *J. Geophys. Res.* 82, 4351–4363.
- Kallio, E., Koskinen, H., Barabash, S., Lundin, R., Norberg, O., Luhmann, J.G., 1994. Proton flow in the martian magnetosheath. *J. Geophys. Res.* 99, 23547–23599.
- Karlsson, E., Fedorov, A., Barabash, S., the Aspera-3 team, 2006. Mass composition of the escaping plasma at Mars, implications for carbon inventory. *Icarus* 182, 320–328.
- Kerr, R., Wetter, A., 2000. Younger Mars emerging. *Science* 289, 714–716.
- Krymskii, A.M., Breus, T.K., Ness, N.F., Acuña, M.H., Connerney, J.E.P., Crider, D.H., Mitchell, D.L., Bauer, S.J., 2002. Structure of the magnetic field fluxes connected with crustal magnetization and topside ionosphere at Mars. *J. Geophys. Res.* 107 (A9), doi:10.1029/2001JA000239. 1245.
- Luhmann, J.G., Bauer, S.J., 1992. Solar wind effects on atmospheric evolution at Venus and Mars. In: *Venus and Mars: Atmospheres, Ionospheres, and Solar Wind Interactions*. AGU Monograph, vol. 66, pp. 417–430.
- Luhmann, J.G., Schwingenschuh, K., 1990. A model of the energetic ion environment of Mars. *J. Geophys. Res.* 95, 939–945.
- Lundin, R., Dubinin, E.M., 1992. Phobos-2 results on the ionospheric plasma escape from Mars. *Adv. Space Res.* 12 (9), 255.
- Lundin, R., Zakharov, A., Pellinen, R., Hultqvist, B., Borg, H., Dubinin, E.M., Barabash, S., Pissarenko, N., Koskinen, H., Liede, I., 1989. First results of the ionospheric plasma escape from Mars. *Nature* 341, 609–612.
- Lundin, R., Zakharov, A., Pellinen, R., Barabash, S.V., Borg, H., Dubinin, E.M., Hultqvist, B., Koskinen, H., Liede, I., Pissarenko, N., 1990. ASPERA/Phobos measurements of the ion outflow from the martian ionosphere. *Geophys. Res. Lett.* 17, 873.
- Lundin, R., Dubinin, E.M., Barabash, S.V., Koskinen, H., Norberg, O., Pissarenko, N., Zakharov, A.V., 1991. On the momentum transfer of the solar wind to the martian topside ionosphere. *Geophys. Res. Lett.* 18, 1059.
- Lundin, R., Barabash, S., Andersson, H., Holmström, M., the ASPERA-3 team, 2004. Solar wind induced atmospheric erosion at Mars—First results from ASPERA-3 on Mars Express. *Science* 305, 1933–1936.
- McElroy, M.B., Kong, T.Y., Yung, Y.L., 1977. Photochemistry and evolution of Mars' atmosphere: A Viking perspective. *Geophys. Res.* 82, 4379–4388.
- Melosh, H.J., Vickery, A.M., 1989. Impact erosions of the primitive atmosphere of Mars. *Nature* 338, 487–489.
- Mitchell, D.L., Lin, R.P., Mazelle, C., Rème, H., Cloutier, P., Connerney, J., Acuña, M., Ness, N., 2001. Probing Mars' crustal magnetic field and ionosphere with the MGS electron reflectometer. *J. Geophys. Res.* 106, 23419–23428.
- Moore, T.E., Lundin, R., Alcayde, D., Andre, M., Ganguli, S.B., Temerin, M., Yau, A., 1999. Source processes in the high-latitude ionosphere. *Space Sci. Rev.* 88, 7–84.
- Nier, A.O., McElroy, M.B., 1977. Composition and structure of Mars' upper atmosphere: Results from the neutral mass spectrometers. *J. Geophys. Res.* 82, 4341–4350.
- Norberg, O., Lundin, R., Barabash, S., 1993. Observation of molecular ions in the martian plasma environment. In: Gombosi, T.I. (Ed.), *COSPAR Colloquium 4, "Plasma Environments of Non-Magnetic Planets,"* pp. 299–304.
- Paschmann, G., Haaland, S., Treumann, R. (Eds.), 2002. *Auroral Plasma Physics*. *Space Sci. Rev.* 103, 1–4.
- Pérez-de-Tejada, H., 1987. Plasma flow in the Mars magnetosphere. *J. Geophys. Res.* 92, 4713.
- Pérez-de-Tejada, H., 1998. Momentum transport in the solar wind erosion of the Mars ionosphere. *J. Geophys. Res.* 103, 31499–31508.
- Pérez-de-Tejada, H., 2005. Empirical values of the transport coefficients of the solar wind: Conditions in the Venus ionosheath. *Astrophys. J.* 618 (2), L145–L148.
- Phillips, J.L., Luhmann, J.G., Russell, C.T., Moore, K.R., 1987. Finite Larmor radius effect on ion pick-up at Venus. *J. Geophys. Res.* 92, 9920–9930.
- Russell, C.T., Luhmann, J.G., Schwingenschuh, K., Riedler, W., Yeroshenko, Ye., 1990. Upstream waves at Mars: Phobos observations. *Geophys. Res. Lett.* 17, 897.
- Sauer, K., Dubinin, E., 2000. The Nature of the martian 'obstacle boundary'. *Adv. Space Res.* 26 (10), 1633–1637.
- Shefer, R.E., Lazarus, A.J., Bridge, H.S., 1979. A reexamination of plasma measurements from the Mariner 5 Venus encounter. *J. Geophys. Res.* 84, 2109–2114.
- Shapiro, V.D., Szegő, K., Ride, S.K., Nagy, A.F., Shevchenko, V.I., 1995. On the interaction between the shocked solar wind and the planetary ions on the dayside of Venus. *J. Geophys. Res.* 100, 21289–21306.
- Slavin, J.A., Intriligator, D.S., Smith, E.J., 1989. Pioneer Venus orbiter magnetic field and plasma observations in the Venus magnetotail. *J. Geophys. Res.* 94, 2383–2398.
- Trotignon, J.G., Grard, R., Barabash, S., Lundin, R., Dubinin, E., 1996. Solar wind measurements near Mars and their implication in the red planet environment. *Planet. Space Sci.*, 117–127.
- Winningham, J.D., Frahm, R.A., Sharber, J.R., Coates, A.J., Linder, D.R., Soobiah, Y., Kallio, E., Espley, J.R., Barabash, S., Lundin, R., the Aspera-3 team, 2006. Electron Oscillations in the martian Magnetosphere. *Icarus* 182, 360–370.
- Verigin, M.I., Shutte, N.M., Galeev, A.A., Gringauz, K.I., Kotova, G.A., Remizov, A.P., Rosenbauer, H., Hemmerich, P., Livi, S., Richter, A.K., Apathy, I., Szego, K., Riedler, W., Schwingenschuh, K., Steller, M., Yeroshenko, Ye.G., 1991. Ions of planetary origin in the martian magnetosphere (Phobos 2/TAUS experiment). *Planet. Space Sci.* 39, 131–137.
- Vignes, D., Mazelle, C., Rème, H., Acuña, M.H., Connerney, J.E.P., Lin, R.P., Mitchell, D.L., Cloutier, P., Crider, D.H., Ness, N.F., 2000. The solar wind interaction with Mars: Locations and shapes of the bow shock and the magnetic pile-up boundary from the observations of the MAG/ER experiment onboard Mars Global Surveyor. *Geophys. Res. Lett.* 27, 49–52.